ELSEVIER

Journal of Atmospheric and Solar-Terrestrial Physics ▮ (▮▮▮▮) ▮▮▮–▮▮▮

Journal of ATMOSPHERIC AND SOLAR-TERRESTRIAL PHYSICS

www.elsevier.com/locate/jastp

Evidence of mesospheric bore formation from a breaking gravity wave event: simultaneous imaging and lidar measurements

S.M. Smith[a,*], J. Friedman[b], S. Raizada[b], C. Tepley[b], J. Baumgardner[a], M. Mendillo[a]

[a]*Center for Space Physics, Boston University, 725 Common wealth Avenue, Boston, MA 02215, USA*
[b]*National Astronomy and Ionosphere Center, Arecibo Observatory, Arecibo, PR 00612, USA*

Received 22 January 2004; received in revised form 9 September 2004; accepted 16 November 2004

Abstract

A large wave event was observed in the three upper-mesospheric (80–105 km) airglow emissions of O(^{1}S), Na and OH by the Boston University all-sky imager, at the Arecibo Observatory, during the night of 3 May 2003. The airglow structures appeared to be due to a large upward propagating internal gravity wave, which subsequently became unstable near the 95 km height level and produced large-scale vertical motions and mixing. Simultaneous density and temperature lidar measurements indicated the presence of a large temperature inversion of 80 K valley-to-peak between 88 and 96 km during the time of the event. Near-simultaneous temperature profiles, made by the TIMED SABER instrument, provided evidence that the horizontal extent of the inversion was localized to within 500 km of Arecibo during the wave event. As the gravity wave dissipated, an internal bore was generated, apparently due to the deposition of momentum and energy into the region by the original wave. Although mesospheric gravity wave breaking has been reported previously (Swenson and Mende, 21(1994); Hecht et al., 102(1997); Yamada et al., 28(2001), for example), this was the first time that the phenomenon has been associated with the generation of an internal mesospheric bore. The event suggested that the breaking of a large mesospheric gravity wave can lead to the generation of an internal bore, as suggested by Dewan and Picard 106(2001). Such behavior is of particular interest since little is known of their origins.

Keywords: Mesophere; Dynamics; Gravity waves; Airglow; All-sky Imaging; Lidar

1. Introduction

The vertical temperature and wind structure of the upper mesosphere and lower thermosphere can create the conditions suitable for the trapping and ducting of gravity waves (Walterscheid et al., 1999). Such ducts can allow the transportation of gravity wave momentum and energy over large distances, a characteristic that has important consequences for momentum and energy transport in the upper atmosphere. All-sky imagers regularly record quasi-monochromatic (QM) gravity wave activity in the various night-time mesospheric emissions (e.g., Taylor et al., 1995a; Wu and Killeen, 1996; Hecht et al., 1997; Swenson et al., 1999; Smith et al., 2000). Several studies have shown that a significant proportion of these waves are ducted or evanescent

*Corresponding author. Tel.: +1 001 617 353 6658; fax: +1 001 617 353 6463.
E-mail address: smsm@bu.edu (S.M. Smith).

1364-6826/$ - see front matter © 2005 Elsevier Ltd. All rights reserved.
doi:10.1016/j.jastp.2004.11.008

(~75% (Isler et al., 1997); ~55% (Smith et al., 2000), for example). In the study by Walterscheid et al. (1999), it was suggested that all observed QM waves are ducted.

While QM mesospheric gravity waves are omni-present in routine all-sky images of the mesosphere, there is a distinct class of uncommon events—sudden, frontal all-sky airglow emission enhancements or depletions followed by a series of propagating waves that are phase-locked to the leading front and lasting 1–2 or more hours. Very few cases have been reported in the literature and they appear to consist of two distinct types of disturbances. The first type is known as a "wall" event. This type appears to be due to a large freely propagating gravity wave which becomes unstable and then produces overturning and mixing of the airglow layers. One example occurred during the ALOHA campaign in Hawaii (Swenson and Espy, 1995; Swenson et al., 1998) and another in Brazil (Medeiros et al., 2001; Batista et al., 2002).

The other type is the bore event. A bore consists of a propagating step-like disturbance followed by either a series of propagating phase-locked wave-crests (an undular bore) or an extended turbulent region (a turbulent bore). Atmospheric bores require a stable region in which to propagate and they can travel large distances without significant attenuation. The existence of bores on rivers (e.g., Tricker, 1965 Lighthill, 1978), in oceans (e.g., Osborne and Burch, 1980; Apel et al., 1985) and in the lower atmosphere (e.g., Smith, 1988; Mahapatra et al., 1991) has long been established. Their existence in the mesosphere, however, has only been recently reported. It was Dewan and Picard (1998) who first suggested that an unusual wave event observed by Taylor et al. (1995b) was a mesospheric bore. In the mesosphere, a temperature inversion or perhaps a vertical wind shear, would provide a stable ducting region for the propagation of a bore.

The normalized bore strength describes the size of a bore disturbance and is defined as $\beta = (h_1 - h_0)/h_0$, where h_0 and h_1 are the respective depths of the duct prior to and during the passage of the bore disturbance and the duct depth $= 2h_0$. A bore strength of $\beta < 0.3$ tends to result in an undular bore, and if $\beta > 0.3$, in turbulent behavior (see Lighthill, 1978), although, in practice, this limit is not held rigorously.

There have been only a few reports of mesospheric bore activity in the literature. For example, Smith et al. (2003) presented comprehensive evidence indicating that what appeared to be a large naked-eye gravity wave was actually a large undular bore that had propagated a horizontal distance of over 1200 km. A temperature inversion was shown to be present during the time of the event, although not directly over the imager site. She et al. (2004) has reported recently on observations of a co-located bore and temperature inversion. The bore in question was initially undular, and was observed to change into a turbulent bore during the event. Loughmiller et al. (2004) presented evidence of the existence of multiple bores due to the presence of multiple ducting regions in the mesosphere. While wall events and bores are a different phenomena, they both exhibit similar appearances in all-sky images, i.e., a sudden frontal onset with trailing wave-fronts. In a study of 12 frontal and wave train events at Millstone Hill (Smith, 2002) it was found that 10 of the events were large vertically propagating or ducted gravity waves and that only two were bores. The Millstone events showed that information about the vertical structure of the wave field is crucial in order to determine the nature of a wave disturbance that may appear, superficially, to be a bore.

This paper will present and discuss co-located multi-diagnostic observations of a wave event that was recorded by an all-sky imager and Na and K resonance lidars at Arecibo on the night of 3 May 2003.

2. Observations and analysis

The Boston University all-sky imaging system (Baumgardner et al., 1993; Smith et al., 2000) has been operating at Arecibo since May 2002. It utilizes a bare 1024×1024-pixel charge-coupled device cooled to $-50\,^{\circ}\mathrm{C}$. A rotating filter-wheel houses up to six narrow-band (1.2–1.8 nm FWHM) filters, three of which record the night-time mesospheric emissions: O(^{1}S) near 96 km in altitude (557.7 nm), Na near 90 km (589.3 nm), and the OH Meinel bands in the near-infrared (695–950 nm) originating from near 87 km. Of the remaining three, one filter centered at 644.4 nm is used to monitor continuum emission and another position houses a dark filter position for calibration purposes. The sixth position has a O(^{1}D) (630.0 nm) filter for thermospheric studies.

Images are processed as follows: (1) The numerous stars in the images were removed using a numerical algorithm. (2) The images were then corrected for vignetting by the optical system and for line-of-sight viewing effects, such as van Rhijn brightening near the horizon. (3) The images were corrected geometrically for distortion by the lens system (unwarped) and mapped to the assumed layer heights above the Earth's surface.

Fig. 1 shows three unwarped all-sky images in (a) O(^{1}S), (b) Na, and (c) OH emission taken after the wave event passed through the zenith. The waves propagated in the direction of 20° east of north (denoted by the arrow in Fig. 1) with the leading wave-front having an observed phase speed (c_{obs}) of $62 \pm 2\,\mathrm{ms}^{-1}$. The average horizontal wavelength (λ_{h}) of the three leading waves in the train was 27.7 ± 1.4 km and the observed period of the waves was 8.0 ± 0.8 min.

The disturbance was characterized by an initial brightness increase/decrease in the O(^{1}S)/OH emissions followed by series of phase-locked waves, which is

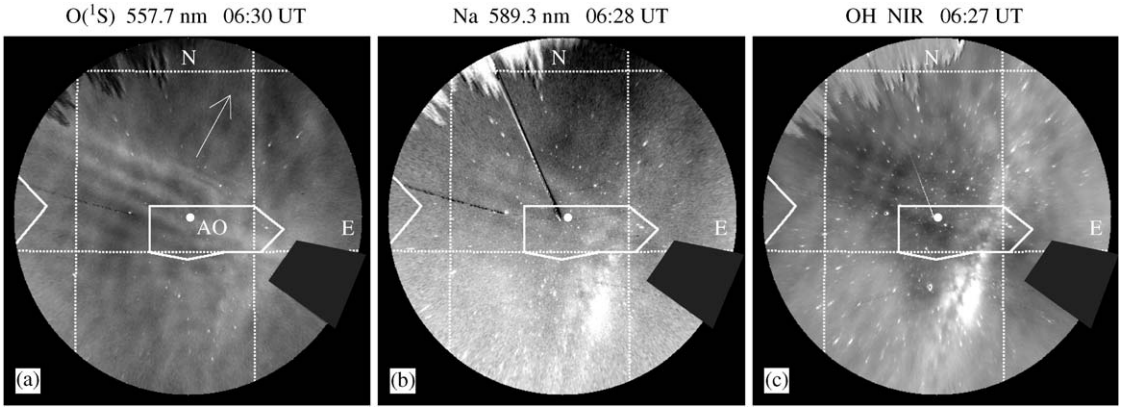

Fig. 1. Unwarped all-sky images in (a) O(^{1}S), (b) Na, and (c) OH emission of the wave disturbance recorded on 3 May 2003 at Arecibo Observatory (marked as "AO" and its position is marked with an asterisk). The direction of the waves is shown by the arrow. The broad feature in the lower right part of the Na and OH images is the Milky Way. The dark feature in the south–east of the images is a light shade, and the faint dark line extending from the NW towards the center of the Na and OH images is one of the lidar beams.

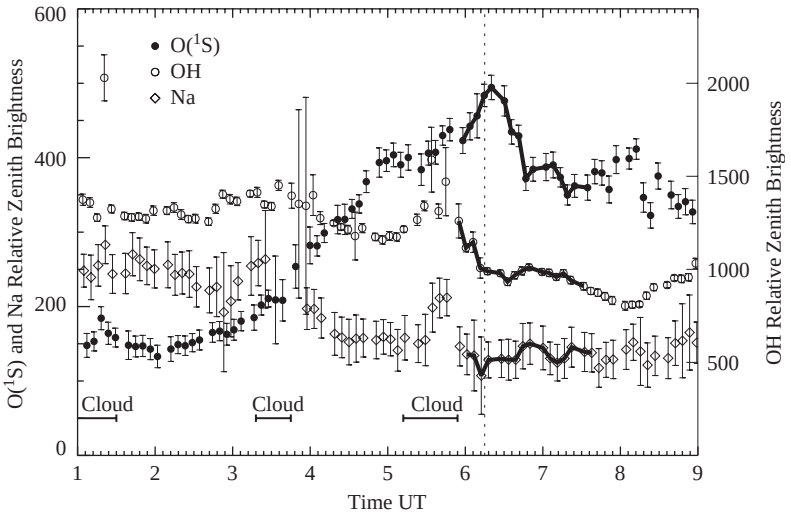

Fig. 2. Time histories of the zenith brightness in the O(^{1}S) (solid circles), OH (open circles), Na (open diamonds) emissions on 3 May 2003. The zenith crossing time of the leading wave-front at 06:15 UT is marked with the vertical dashed line. The brightness values for the time period during the event are connected together. Periods of cloud are marked with solid horizontal bars.

consistent with a wall-type event. The wave patterns were most evident in the O(^{1}S) emission and least so in the Na images. The intensity amplitude of the waves was not unusually large—the amplitude in the OH emission, for example, was only 2.7% above the mean emission level, which is typical for mesospheric gravity wave events. The wall event reported by Swenson and Espy (1995) exhibited an amplitude of ~30%. Further, although the wave-fronts extended across the entire sky, only three wave-fronts were associated with the initial gravity wave.

The zenith brightness time histories for the three emissions are shown in Fig. 2. These were obtained by sampling the mean brightness values over a 7×7 pixel square (2.1 km × 2.1 km at 90 km altitude) centered on the zenith. The error bars are the standard deviations associated with the mean brightness. Periods of cloud interference during the night are denoted by the horizontal bars. The effect of clouds (and also stars) was to increase the mean brightness values and the associated standard deviation. This effect can be seen in Fig. 2 occurring just prior to 06:00 UT. The 557.7 nm emission brightness reached a maximum at 06:22 UT, as the disturbance transited the zenith, and then decreased rapidly during the passage of the wave train.

In addition to the small-scale waves associated with the disturbance, the 557.7 nm emission also exhibited a

large-scale brightness variation over the night with a period of >10 h. The large-scale variation, which was most probably associated with the semi-diurnal tide, propagated towards the NE, in the same direction as the disturbance. Equivalent large-scale variations were not evident in the OH and Na emissions. The brightness of these emissions essentially decreased over the course of the night.

Fig. 3a is a range-time-intensity (RTI) plot of the mesospheric Na density obtained on the night by the Na resonance lidar at Arecibo (Tepley et al., 2003). During 1–2 h prior to the event (vertical dashed line), the densest region of the layer was centered near 94–95 km. At 06:00 UT, the bottom-side of the layer (at ~80 km) increased in height by 2–3 km. The top-side of the layer (at ~100 km) increased in height by 2–3 km as the disturbance passed through the zenith, about 15 min later. In addition, a region of enhanced Na density near 92 km was advected 3–4 km downwards. Another advection event occurred after 08:00 UT when a similar, fainter disturbance passed overhead.

Fig. 4a is an RTI density plot of the mesospheric potassium layer in the 80–105 km region during the night obtained by the K resonance lidar at Arecibo (Friedman et al., 2000, 2003). During the early part of the night until ~5:30–6:00 UT, the layer exhibited a double peak structure centered near 92 and 95 km. After the time of the zenith crossing of the leading wave-front (vertical dashed line) only a broad single layer centered near 93 km was observed. From that time onwards, the top- and bottom-sides of the layer increased in height by 3–4 km. A small (~1 km) downward extension of enhanced K density occurred near 92 km during the first 15–20 min of the passage of the disturbance, as was seen in the Na layer. A similar extension was also seen around 8 UT. Both the sodium and potassium layers in Figs. 3 and 4a, respectively, exhibit similar behavior due to the passage of the disturbance, namely a height increase in the top-and bottom-sides of the layers and downward advection of both species. The height increase of the top-side of the K layer, was probably broadening due to turbulent mixing as a result of the large-scale instability of the wave. The double-layered structure observed in the potassium density profile (but not in the sodium) during the first half of the night was probably not related to the disturbance itself; however, the double structure appeared to disintegrate into a single layer as a result of the passage of the disturbance.

During the course of the night, both the Na and K layers descended in height at a rate of $\sim 0.3\,\mathrm{ms}^{-1}$. Similar descending layers have been observed in other metals, such as Ca and Ca^+, with downward phase velocities of $1.0–2.5\,\mathrm{ms}^{-1}$. These have been attributed to the downward semi-diurnal tidal phase velocity and are often seen at Arecibo (Tepley et al., 2003; Matthews and Bekeny, 1979).

Fig. 4b shows the 12-min averaged temperature field of the mesopause region. A temperature maximum was present which descended at $\sim 0.6\,\mathrm{ms}^{-1}$ from above 100 km down to 90 km during the course of the night. Interestingly, during the same period, the temperature minimum lying below the maximum region, descended from 95 to 87 km at a rate of $\sim 0.4\,\mathrm{ms}^{-1}$, similar to the metal densities shown above. The mesospheric temperature variation at the 95–97 km height level during the night was well correlated with the $O(^1S)$ emission brightness variation during the course of the night (Fig. 2).

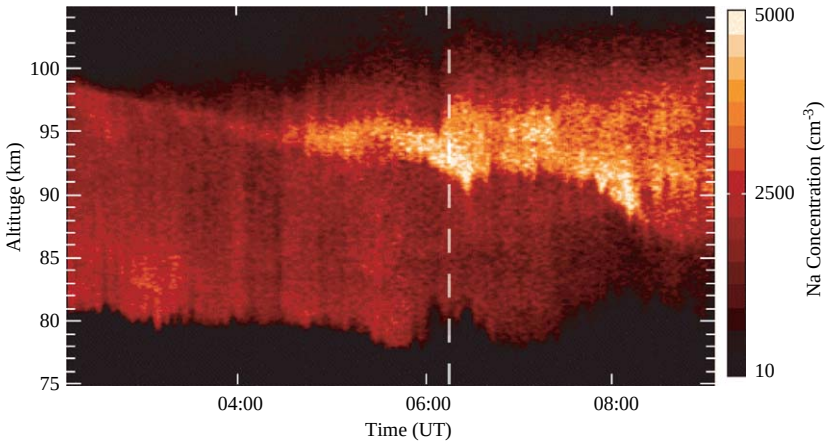

Fig. 3. Sodium RTI density profile in the 80–105 km height region made on the night of 3 May 2003 with the Na resonance lidar at the Arecibo Observatory. The vertical dashed white line denotes the time of the zenith transit of the leading wave-front. The downward extension of the densest region just after this time is evidence of large-scale downward advection as the wave passed over the site. A similar feature is seen just after 8 UT when a similar but fainter disturbance passed overhead. The top-side of the layer exhibited substantial broadening after 06:15 UT due to turbulence and mixing as the wave became unstable.

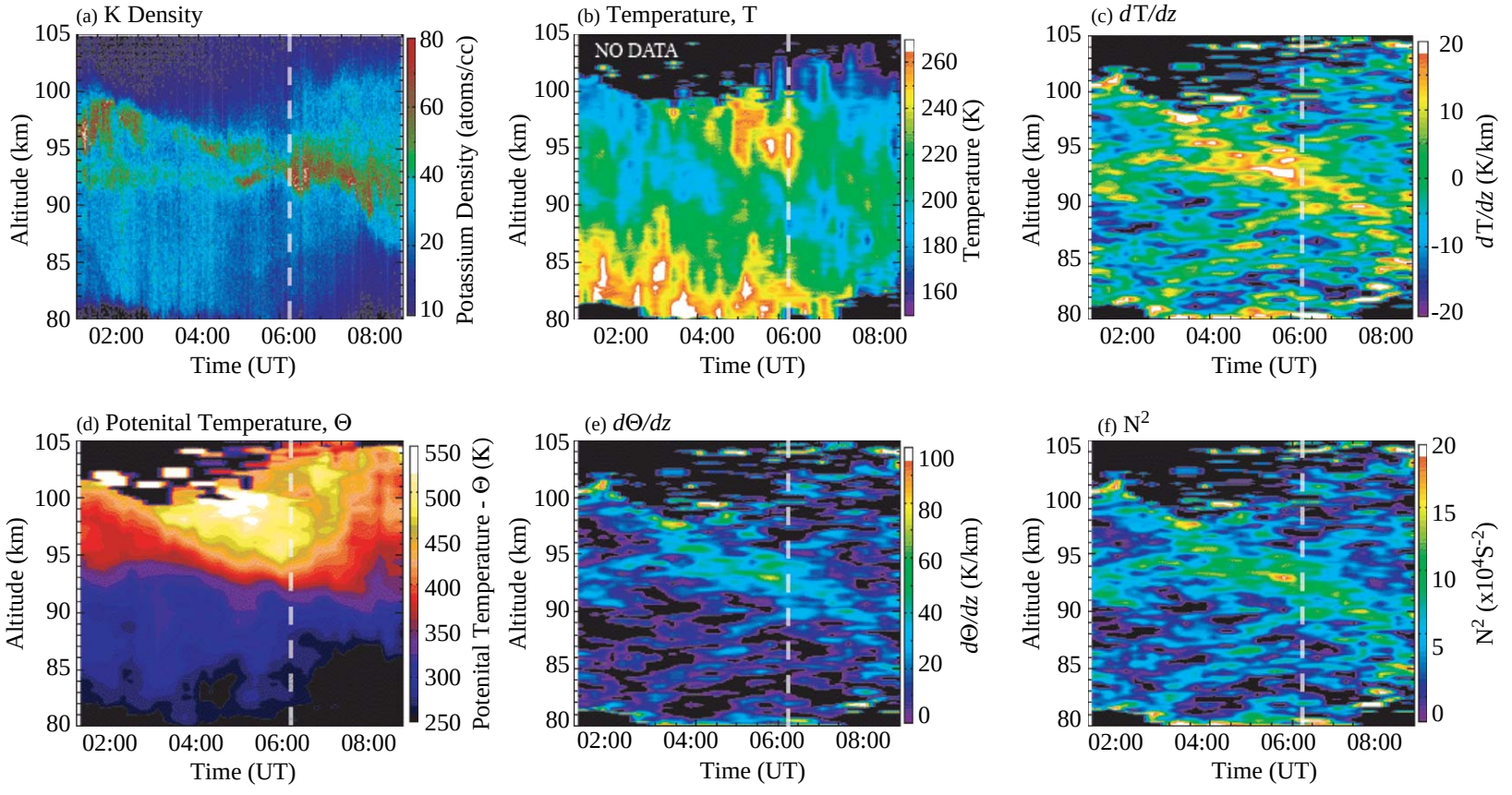

Fig. 4. Potassium lidar measurements of the 80–105 km height region on the night of 3 May 2003 made at Arecibo Observatory. Shown is the RTI profile of (a) K density, along with contour profiles of (b) temperature (T), (c) the vertical temperature gradient (dT/dz), (d) potential temperature (Θ), (e) the vertical potential temperature gradient ($d\Theta/dz$), and (f) the square of the Brünt-Vaisala frequency (N^2). The profiles in Panels (c–f) were derived from the temperature measurements in Panel (b). The vertical dashed white line denotes the zenith crossing time of the leading wave-front. The solid bars above each panel denote periods of partial cloud cover. The cloud did not have a serious impact on the data quality.

The zenith transit of the gravity wave event coincided with a large, transient temperature enhancement centered near 95–96 km, which can be seen in Fig. 4b. The enhanced temperature reached a maximum of ~265 K and lasted for about 20 min. At that time, the temperature inversion was 80 K valley-to-peak and it extended over 8 km from 88 to 96 km. In addition, the lapse rate in the 80–90 km and 95–100 km height regions prior to, and during, the first hour of the event was super-adiabatic (i.e., $dT/dz < -9.5\,K\,km^{-1}$) (as shown in Fig. 4c), so the region was convectively unstable. The large-scale temperature maximum began to disappear after 06:30 UT, probably due to large-scale advection that occurred as the wave became unstable and the broke, as evidenced further in Fig. 4d.

Fig. 4d shows the contours of potential temperature, $\Theta(z,t)$, calculated from the temperature field in Fig. 4b. For a fluid in hydrostatic equilibrium, $\Theta(z,t)$ increases with height and contours of equal $\Theta(z,t)$ are horizontal. Particularly noteworthy in Fig. 4c are the vertical contours of $\Theta(z,t)$ that occurred above 94 km during 06:30–07:30 UT. This behavior is evidence of large-scale adiabatic vertical motion (of 6–8 km in extent). Similar behavior in the potential temperature during breaking gravity wave events has been reported previously from Na lidar temperature measurements (Williams et al. (2002) and Franke and Collins (2003), for example). It should be noted that the downward advection of enhanced Na and K seen in Figs. 3 and 4a occurred just prior to the upward advection exhibited in Fig. 4d. This upward motion can also be seen in Figs. 3 and 4a.

Fig. 4f is a contour plot of the square of the Brünt-Vaisala frequency (N^2) in the 80–105 km height region, derived from the temperature measurements in Fig. 4b. The contours have been smoothed over a vertical height of 2 km. A narrow region, about 4–7 km deep and allowing propagating wave modes ($N^2 > 0$) with periods larger than ~4–5 min, descended at $\sim 0.5\,ms^{-1}$ during the night from 100 to 85 km. Between 05:00 and 07:00 UT, the region was centered near 93 km and could have provided a suitable ducting region for wave propagation. Fig. 4f also indicates that waves with periods greater than about 4–5 min would have been able to propagate into the 80–100 km height region from below during the course of the night—the original wave period was 8.0 min. However, a narrow region at the 85–87 km level, allowing only waves with periods of greater than about 8–9 min to freely propagate, occurred after 05:00 UT. As a result, and with the effect of local winds (not taken into account in Fig. 4f), the narrow region probably contributed to the wave becoming unstable and breaking.

The time evolution of the vertical phase structure of the disturbance in the three emissions was especially striking, and is shown in Fig. 5. Each panel is a set of cross-sectional plots (slices) made through three unwarped images, closely spaced in time. The panels are separated in time by approximately 10 min and are named with the average time of the images. The slices were made in the direction of propagation and they have been horizontally shifted, using the deduced speed of the leading wave-front, in order to account for the acquisition time differences between each image. The slices have also been separated vertically to represent the heights and relative separations of the emission layer centers. The O(^{1}S) layer was assumed to be centered nominally at 96 km. The Na layer was centered near 93.5 km in altitude at the onset of the event (Fig. 3). The OH layer was centered at 85 km and exhibited a FWHM thickness of 11 km. The OH layer height was obtained from measurements by the Sounding of the Atmosphere Broadband Emission Radiometry (SABER) instrument (Mertens et al., 2001, 2004) aboard the NASA TIMED satellite which passed within 300–400 km of the Arecibo Observatory on 3 May at 06:25–06:30UT (discussed below). There was other unrelated gravity wave activity during the course of the night, in the OH emission in particular, which would have altered minor features of the cross sections.

Initially, between 06:00 and 06:30 UT, the disturbance exhibited a vertical structure consistent with a large upward propagating gravity wave. This is particularly evident in Fig. 5b where a visual fit of lines of constant phase have been drawn over the slices. The variation in the slope of the phase lines indicates that the vertical wavelength of the gravity wave varied with altitude, from ~18 to 45 km. The variation is most probably caused by a vertical shear in the background wind.

After 06:30 UT, wave-fronts #1 and #2 began to disappear and a bore-like vertical structure (Taylor et al., 1995b; Smith et al., 2003), with the leading wave-front associated with wave-front #3 of the original disturbance, began to form in the O(^{1}S) and OH emissions (its position is indicated by the vertical dashed lines in Figs. 5c–f). The O(^{1}S)/OH emission intensity decreased/increased behind the leading wave-front (in this case wave-front #3) in a manner typical of what one might expect from a bore propagating at a height between the two layers. Wave-front #3 was phase-locked to exactly 180° in the OH and O(^{1}S) emissions, and it was in-phase in the Na and O(^{1}S) emissions (Figs. 5c–f). In addition, a stable ducting region, necessary for bore propagation, was centered near 93 km during the time of the event (Fig. 4d). The trailing waves were well defined in the O(^{1}S) emission but, in the OH emission, only a trailing turbulent region was observed behind the front, indicating that the bore disturbance was undular and turbulent at two different heights (85 and 96 km) simultaneously. Such behavior has not been observed before and it suggests that the propagation conditions in the 85–95 km height region were not uniform, probably due to the presence of a wind shear. In addition, the bore

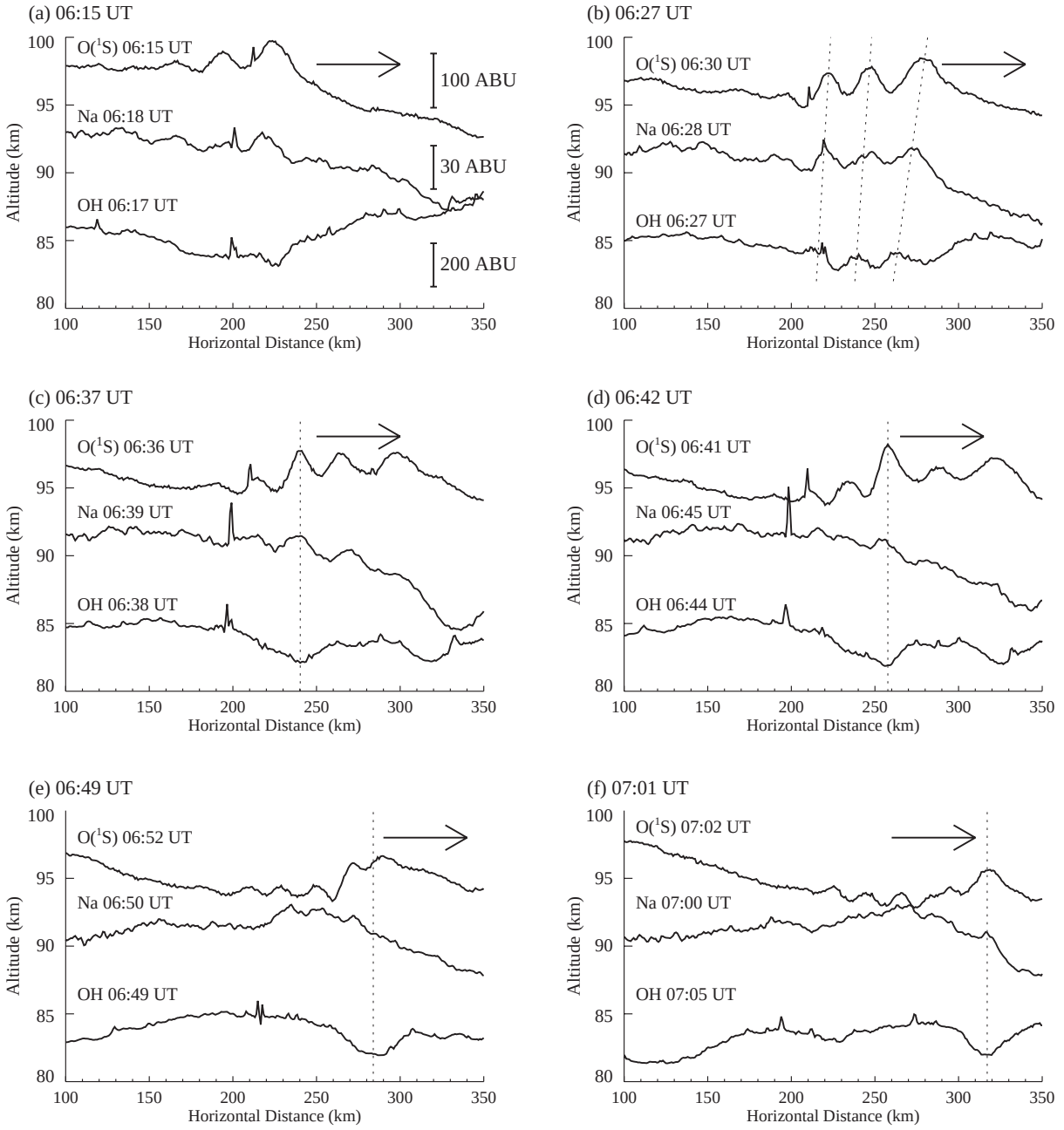

Fig. 5. A series of image cross-sections (slices) of the O(^{1}S), Na and OH emissions along the wave's horizontal propagation direction (arrow) for six time periods separated by about 10 min. The slices have been separated vertically in order to represent the relative vertical separations of the layers in the mesosphere. The slices have also been horizontally shifted using the deduced horizontal wave speed in order to make a quasi-simultaneous "snapshot" of the vertical structure of the wave field. The emission brightness is given in arbitrary brightness units (ABU) in panel (a) and refers to all six panels.

in the OH emission exhibited a group velocity of 53 ms^{-1}, whereas in the O(^{1}S) emission, the group velocity was 36 ms^{-1}.

By 06:50 UT, the original gravity wave event (the wall event) had largely dissipated. At that time, the bore exhibited a horizontal extent of about 150 km (see the OH cross-sections in Figs. 5e and f). By 07:25 UT, the bore had dissipated, having lasted about 1 h (the shortest bore lifetime yet recorded).

3. Results and discussion

An internal gravity wave which is propagating upward (downward) will exhibit a downward (upward) phase progression. The initial phase relationship of the wave-fronts in the three emissions (see Figs. 5a and b) was consistent with a wall-type disturbance, i.e., a large upward-propagating internal gravity wave. The ALOHA wall event (Swenson and Espy, 1995; Swenson et al., 1998) and the event at Cachoeira Paulista, Brazil (Medeiros et al., 2001; Batista et al., 2002) are examples. The transient temperature enhancement that occurred at 06:15 UT near 95–96 km and coincided with the disturbance (Fig. 4b) was very similar to the behavior observed near 91 km during the ALOHA wall event. Both enhancements lasted for 20–25 min, however, the Arecibo event was slightly larger (20–25 K) compared to that during the ALOHA event (15 K). An enhancement in Na column abundance and an increase in the layer height also occurred in all three events. A larger increase was observed in the Arecibo event.

Although the initial vertical phase relationship of the wave-fronts was consistent with an upward-propagating gravity wave, the reason for the phase of the dark leading wave-front of the OH emission is not clear. Its phase difference with the O(^{1}S) emission was initially $\sim 180^\circ$ with the OH slightly leading. Over the course of the event, the phase difference between the emissions increased. One possible reason is that a shear in the local wind field may have altered the vertical wavelength of the disturbance in the region of the layer height during the initial period of the event.

As described earlier, after 06:30 UT, the gravity wave became unstable and generated large-scale vertical motions and mixing, as indicated by the vertical contours in $\Theta(z,t)$ above 94 km (Fig. 4d). The Na and K layers were also displaced upwards in height. As the wave underwent breaking, and deposited its momentum and energy into the local medium, a bore-like vertical structure appeared to form, with wave-front #3 becoming the leading edge. The bore disturbance was centered near 93 km.

Although it is quite possible that the bore disturbance occurred coincidently during the wall event, there were several facts that support its formation as a result of the demise of the latter. Firstly, the bore exhibited a similar speed and azimuth as the original wave event. Fig. 6a shows plots of the positions of the observed bright wave-fronts in the O(^{1}S) (filled circles), Na (asterisks) and OH (open circles) emissions during the night. The measurement uncertainty of the wave-front positions was 0.9 km. Wave-fronts #1–3 were associated with the original wave event and wave-fronts #3–8 were associated with the internal bore disturbance. During the initial appearance of the bore, wave-front #3 broadened markedly for a time. The extent of the broadening is shown as the bold vertical lines near 06:45 UT in Fig. 6a. Wave-front #3 was also the longest-lived of the wave-fronts. The linear fits indicated that the phase speed of each wave-front was constant during the course of the event.

There was no significant discontinuity in the wave-front positions or speeds indicated in Figs. 6a and b at the time of the appearance of the bore feature. Such a discontinuity would be expected if the bore disturbance had formed independently and then subsequently overtaken the wall event as it propagated through the upper mesosphere. Also, and very importantly, an inversion layer capable of supporting a ducting region,necessary for bore propagation, was present at the time of the event (see Fig. 4b). Therefore, our conclusion is that the bore originated from the breaking of the original gravity wave disturbance.

During the entire course of the event, the leading wave-fronts in O(^{1}S) and OH emissions exhibited larger amplitudes and phase speeds than the trailing ones (known as amplitude ordering). The phase speeds of the wave-fronts are plotted in Fig. 6b. In the O(^{1}S) emission for example, the phase speed of the leading three wave-fronts associated with the wall event ranged from 62 ms^{-1} for the leading wave-front (61 ms^{-1} in the OH emission) down to 53 ms^{-1} for wave-front #3. This nonlinear behavior is a result of the larger amplitude waves propagating faster than the smaller ones and has been observed previously in internal bores (Mahapatra et al., 1991; Smith et al., 2003, for example). The amplitude ordering was not as clearly exhibited in the Na emission, possibly due to the relative faintness of the wave patterns in the Na images.

The phase speeds of the wave-fronts associated with the bore exhibited a less marked decrease compared to those in the wall event and appeared to increase in the final trailing wave-fronts (#7 and #8).

The mean horizonta1 wavelength of the wave-fronts (λ_h) associated with the initial gravity wave event decreased with increasing rank (see Fig. 6c). For a given wave-front, the wavelength tended to decrease over time and during the course of the event. The exception to this was the wavelength between wave-fronts #1 and #2, which increased over time (mean of 29.3 km). The mean horizontal wavelength associated with the gravity wave (the wall event) (wave-fronts #1–3) was 27.7 ± 1.4 km. The mean horizontal wavelength associated with the bore disturbance (wave-fronts #4–8) was significantly less: $\lambda_h = 21.8 \pm 2.9$ km. The uncertainties were the standard deviations ($\pm\sigma$).

A ducting region of depth 7 km (FWHM) ($= 2h_0$), the existence of which is necessary for bore propagation, occurred during the event (see Fig. 4f). Using the model developed by Dewan and Picard (1998) and setting the upper limit of $\beta = 0.3$ for the undularity condition, this bore would be expected to exhibit a horizontal phase

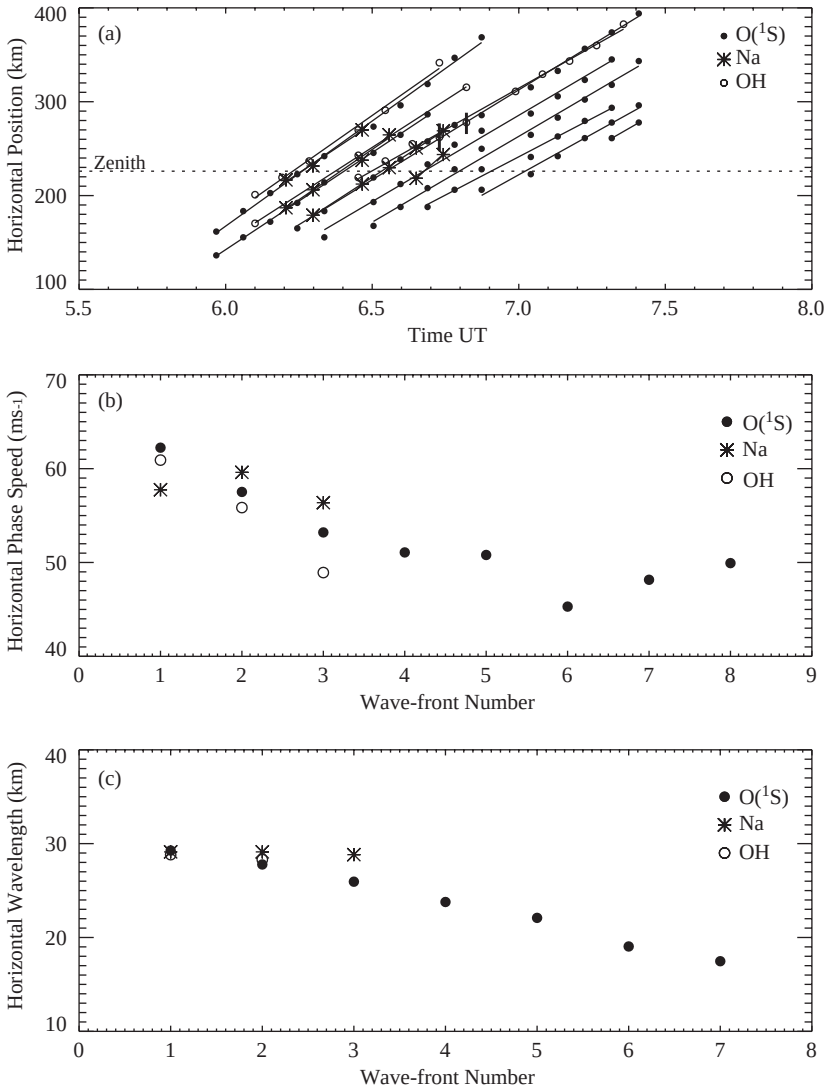

Fig. 6. (a) The measured positions of the bright wave-fronts of the disturbance in the O(^{1}S) (filled circles), Na (asterisks) and OH (open circles) emissions. The vertical bars associated with the OH measurements at ~06:45 UT indicate the horizontal extent of wave-front #3 at that time. (b) Plot of the horizontal phase speeds of the individual wave-fronts in Fig. 6a. The leading wave-fronts propagated faster (~60 ms^{-1}) than those trailing (~45 ms^{-1}), a clear signature of non-linear behavior exhibited by the disturbance, and observed previously in internal undular bores (Smith et al., 2003). (c) Plot of the horizontal wavelengths of the individual wave-fronts showing a clear decrease over distance from the leading edge (and also with time).

speed of 56 ms^{-1}. The bore strength transition criterion is not particularly rigorous, so using the observed values of h_0 and λ_h and Eq. (8) from Dewan and Picard (1998), we solved for the parameter h_1 (= 5.2 km) and then estimated a value of $\beta = 0.49$, which inferred a phase speed of 62 ms^{-1} for the bore. The measured phase speed of the bore was 53 ms^{-1} in the O(^{1}S) emission (wave-front #3), and 49 ms^{-1} in the OH. The estimates have been made without allowing for the local wind, simply because no measurements were available. Despite the limitation, the estimated speed of the wave-front, although slightly higher than measured, was consistent with a bore disturbance. Further, the measured speed was also similar to those made of bore events reported previously (Taylor et al., 1995b; Smith et al., 2003, and She et al., 2004, for example).

Over the course of the lifetime of the bore (~55 min), the number of wave-fronts in the O(^{1}S) emissions increased from three to seven. The extra waves appeared within the imager field of view and were not merely observed approaching from over the horizon. Wave-fronts #4 and #5 were in existence just prior to the

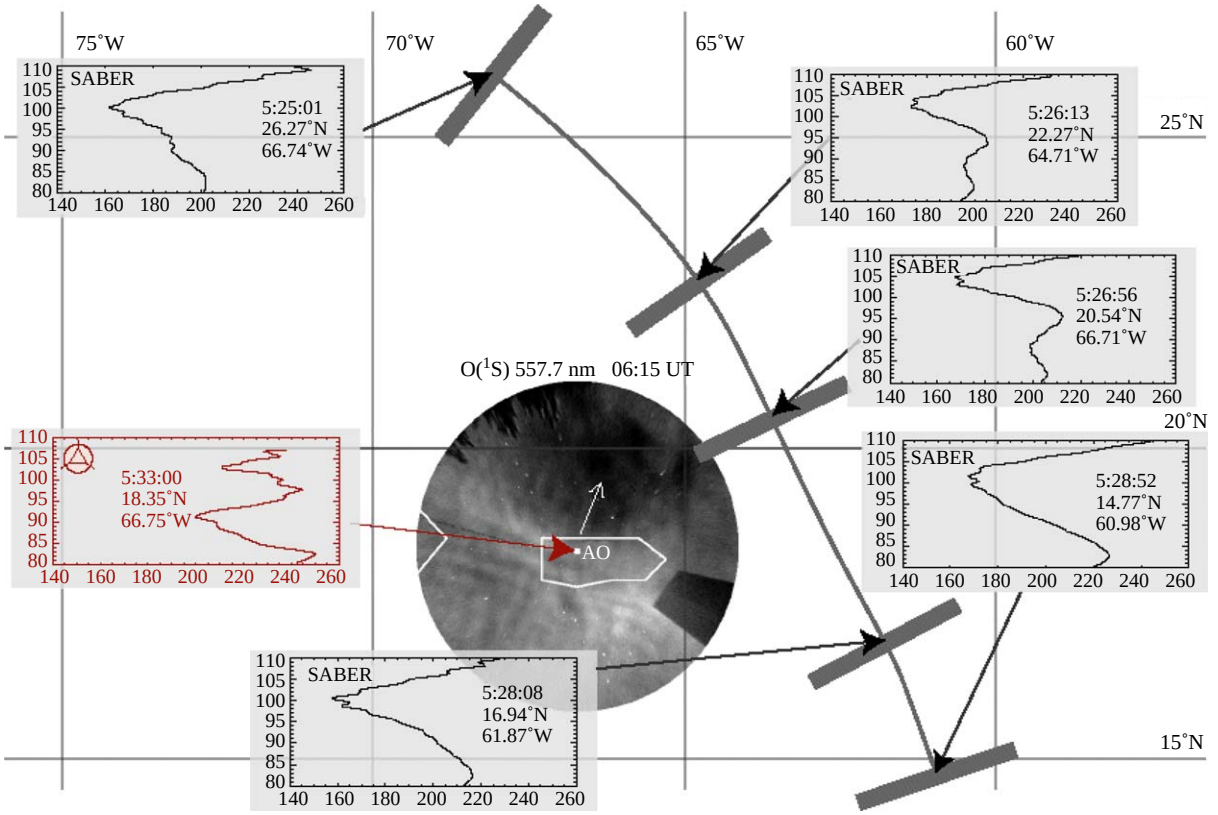

Fig. 7. Map of the Caribbean region showing the relative locations of location of the Arecibo Observatory and the ground-track of the NASA TIMED satellite during an overpass made just prior to the wave event. Five SABER temperature profiles (black), made during the overpass, together with a near-simultaneous temperature profile from the Arecibo K lidar (red), are shown. An overlaid all-sky image, taken during the event, is also shown for scale.

formation of the bore. As a result, the wave addition rate was estimated to be 3 waves h^{-1}, which is only slightly higher than the estimated rates reported for the ALOHA and Texas bore events (2.8 and 1.0 h^{-1}, respectively). The estimated wave addition rate from theory was 1.9 waves h^{-1}.

Dewan and Picard (2001) suggested that mesospheric bores could originate by the critical-layer interaction of a large gravity wave and the local mean wind field, similar to the mechanism that was proposed of the formation of thermal inversion layers in the mesosphere region (Huang et al., 1998). The interaction would provide the force required to launch the bore disturbance into a pre-existing ducting region. Dewan and Picard (2001) estimated that the time of formation of a mesospheric bore could be as little as 1.2 h (72 min). The formation time for the Arecibo bore disturbance, from Fig. 5, was perhaps ~20 min.

Fig. 7 is a map of the Caribbean region with five overlaid SABER temperature profiles (Mertens et al., 2001, 2004) that were obtained during the TIMED fly over at about 05:25 UT, just prior to the event, together with a temperature profile obtained concurrently by the Arecibo K lidar. An unwarped all-sky image showing the scale and orientation of the wave event has been placed at the position of the Arecibo Observatory. The ground track of the satellite is shown as a broad curve. The horizontal areas sampled by the instrument along the flight track, are shown as gray rectangles. A large temperature inversion of 40 K and at a height of 90–97 km can be seen in the Arecibo temperature profile (05:33 UT). The SABER profiles at 05:26:13 and 05:25:56 UT exhibited similar temperature inversions of 10 and 15 K, respectively, both in the 88–95 km height region. Interestingly, there was no evidence of inversions in the other three SABER temperature profiles, which indicates that the ducting region responsible for supporting the bore disturbance was relatively localized to within less than about 500 km region around Arecibo. The relatively localized region may also explain the short lifetime of the bore event. This finding contrasts with the Texas bore (Smith et al., 2003) which exhibited a lifetime of over 6 h. In that case, an inversion layer was observed ~1100 km to the north of the Texas site and appeared to

support the propagation of the disturbance over a distance of more than 1200 km. Taken together, these two events illustrate the spatial variability in the horizontal extent of temperature inversions observed in the upper mesosphere. Furthermore, during these types of wave events, the SABER measurements can provide important and unique information on the horizontal extent of such inversion layers.

No wind measurements were available at Arecibo during the time of the event. Therefore, the intrinsic wave parameters (with respect to the wind) and the effect of the local winds on the propagation characteristics of the event could not be determined. The presence of a local wind would have certainly altered the ducting conditions deduced from the temperature structure. However, wind vector measurements from the 80–105 km height region were made ~1000 km to the south–west of Arecibo by the TIMED Doppler Interferometer (TIDI) instrument (http://tidi.engin.umich.edu), a Fabry-Perot interferometer, after the event at 07:10 UT. The wind measurements are yet to be validated by the TIDI team and so were not available for publication. However, they suggested the presence of a moderate wind shear in the region, which may have altered the vertical phase structure of the disturbance and also initiated instability in the disturbance. The local wind in the 80–105 km height region at that time was generally in the south–west quadrant, opposite to the propagation direction of the disturbance.

4. Conclusion

Imaging and lidar measurements were made of a large mesospheric gravity wave event at the Arecibo Observatory on the night of 3 May 2003. The upward propagating wave was similar to the wall-type event reported by Swenson and Espy (1995). The wave underwent convective instability, resulting in turbulence and mixing, and the subsequent formation of a short-lived bore disturbance. Although gravity wave breaking has been reported previously (Swenson and Mende, 1994; Hecht et al., 1997; Yamada et al., 2001, for example) this was the first time that the generation of a mesospheric bore has been reported. The time evolution of the event suggests that a relationship may exist between wall-type and bore wave disturbances in that, on some occasions, an internal bore may be generated after the original wave breaks and subsequently deposits its momentum and energy into the local medium, as suggested by Dewan and Picard (2001). Further multi-diagnostic imaging, temperature and wind measurements are therefore required to clarify the propagation conditions and environment responsible for gravity wave/mean wind interaction and subsequent bore generation in the mesosphere.

The imaging and lidar measurements presented here have been shown to yield a sufficient amount of information about this event to successfully characterize it, although a more detailed knowledge of the local wind structure in the 80–100 km region would have aided the interpretation. In fact, the event illustrates how crucial knowledge of the vertical phase information of a wave disturbance, together with local temperature and wind measurements, can be in the characterization and interpretation of mesospheric wave events.

Acknowledgements

The authors would like to sincerely thank Mr. Raúl García of the Arecibo Observatory for his efforts in maintaining the health of the Boston University imaging system. The authors are also grateful to Dr. Chris Mertens for providing the SABER data and to Dr. Qian Wu of the TIDI data group at the High Altitude Observatory for providing the preliminary TIDI wind data. This study was supported by the NSF CEDAR Program under Grant ATM 0123064 and by the NSF Aeronomy Program under Grant ATM 0322875. The Arecibo Observatory is operated by Cornell University under a cooperative agreement with the National Science Foundation.

References

Apel, J.R., Holbrook, J.R., Liu, A.K., Tsai, J.J., 1985. The Sulu Sea internal experiment. Journal of Oceanography 15, 1625–1651.

Batista, P.P., Clemesha, B.R., Simonich, D.M., Taylor, M.J., Takahashi, H., Gobbi, D., Batista, I.S., Buriti, R.A., de Medeiros, A.F., 2002. Simultaneous lidar observation of a sporadic sodium layer, a ''wall'' event in the OH and OI5577 airglow images and the meteor winds. Journal of Atmospheric and Solar Terrestrial Physics 64, 1327–1335.

Baumgardner, J., Flynn, B., Mendillo, M., 1993. Monochromatic imaging instrumentation for applications in aeronomy of the earth and planets. Optical Engineering 32 (12), 3028–3032.

Dewan, E.M., Picard, R.H., 1998. Mesospheric bores. Journal of Geophysical Research 103, 6295–6305.

Dewan, E.M., Picard, R.H., 2001. The origin of mesospheric bores. Journal of Geophysical Research 106, 2921–2927.

Franke, P.M., Collins, R.L., 2003. Evidence of gravity wave breaking in lidar data from the mesopause region. Geophysical Research Letters 30 (3), 1155.

Friedman, J.S., Gonzalez, S.A., Tepley, C.A., Zhou, Q., Sulzer, M.P., Collins, S.C., Grime, B.W., 2000. Simultaneous atomic and ion layer enhancements observed in the mesopause region over Arecibo during the Coqui II sounding rocket campaign. Geophysical Research Letters 27, 449–452.

Friedman, J.S., Tepley, C.A., Raizada, S., Zhou, Q.H., Hedin, J., Delgado, R., 2003. Potassium Doppler-resonance lidar for the study of the mesosphere and lower thermosphere at the Arecibo Observatory. Journal of Atmospheric and Solar Terrestrial Physics 65, 1411–1424.

Hecht, J.H., Walterscheid, R.L., Fritts, D.C., Isler, J.R., Senft, D.C., Gardner, C.S., Franke, S.J., 1997. Wave breaking signatures in OH airglow and sodium densities and temperatures 1. Airglow imaging, Na lidar, and MF radar observations. Journal of Geophysical Research 102, 6655–6668.

Huang, T.Y., Hur, H., Tuan, T.F., Li, X., Dewan, E.M., Picard, R.H., 1998. Sudden narrow temperature inversion-layer formation in ALOHA-93 as a critical-layer-interaction phenomenon. Journal of Geophysical Research 103, 6323–6332.

Isler, J.R., Taylor, M.J., Fritts, D.C., 1997. Observational evidence of wave ducting and evanescence in the mesosphere. Journal of Geophysical Research 102, 26301–26313.

Lighthill, M.J., 1978. Waves in Fluids. Cambridge University Press, Cambridge 504pp.

Loughmiller, P.J., Kelley, M.C., DEwan, E.M., Garcia, F.J., Makela, J.J., Smith, S.M., 2004. Sharp front observations of mesospheric bores: further evidence and new cases. Journal of Geophysical Research, under review.

Mahapatra, P.R., Doviak, R.J., Zrnic, D.S., 1991. Multisensor observation of an atmospheric undular bore. Bulletin of the American Meteorological Society 72, 1468–1480.

Matthews, J.D., Bekeny, F.S., 1979. Upper atmospheric tides and the vertical motion of ionsopheric sporadic layers at Arecibo. Journal of Geophysical Research 84, 2743–2750.

Medeiros, A.F., Taylor, M.J., Takahashi, H., Batsista, P.P., Gobbi, D., 2001. An unusual airglow wave event observed at Cachoeira Paulista 23°S. Advances of Space Research 27 (10), 1749–1754.

Mertens, C.J., Mlynczak, M.G., Lopez-Puertas, M., Wintersteiner, P.P., Picard, R.H., Winick, J.R., Gordley, L.L., Russell, J.M., 2001. Retrieval of mesospheric and lower thermospheric kinetic temperature from measurements of CO_2 15 μm Earth limb emission under non-LTE conditions. Geophysical Research Letters 28 (7), 1391–1394.

Mertens, C.J., Schmidlin, F.J., Goldberg, R.A., Remsberg, E.E., Pesnell, W.D., Russell, J.M., Mlynczak, M.G., Lopez-Puertas, M., Wintersteiner, P.P., Picard, R.H., Winick, J.R., Gordley, L.L., 2004. SABER observations of mesospheric temperatures and comparisons with falling sphere measurements taken during the 2002 summer MaCWAVE campaign. Geophysical Research Letters 31, L03105.

Osborne, A.R., Burch, T.L., 1980. Internal solitons in the Andaman Sea. Science 208, 451–460.

She, C.Y., Li, T., Williams, B.P., Tao Yuan, Picard, R.H., 2004. Concurrent OH imager and sodium temperature/wind lidar observations of a mesopause undular bore event over Fort Collins/Platteville, CO. JGR, submitted for publication.

Smith, R.K., 1988. Traveling waves and bores in the lower atmosphere: the 'morning glory' and related phenomena. Earth-Science Review 25, 267–290.

Smith, S.M., Mendillo, M., Baumgardner, J., Clarke, R.R., 2000. Gravity wave imaging from a sub-auroral site: first results from Millstone Hill. Journal of Geophysical Research 105, 27119–27130.

Smith, S.M., 2002. Mesospheric Waves and Bores. Poster CEDAR Workshop, Longwood, CO., 17–21 June.

Smith, S.M., Taylor, M.J., Swenson, G.R., She, C.Y., Hocking, W., Baumgardner, J., Mendillo, M., 2003. A multidiagnostic investigation of the mesospheric bore phenomenon. Journal of Geophysical Research 108, 13–30.

Swenson, G.R., Mende, S.B., 1994. OH emission and gravity waves (including a breaking wave) in all-sky imagery from Bear lake, UT. Geophysical Research Letters 21, 2239–2242.

Swenson, G.R., Espy, P.J., 1995. Observations of 2-dimensional airglow structure and Na density from the ALOHA, October 9, 1993 'storm flight'. Geophysical Research Letters 22, 2845–2848.

Swenson, G.R., Qian, J., Plane, J.M.C., Espy, P.J., Taylor, M.J., Turnbull, D.N., Lowe, R.P., 1998. Dynamical and chemical aspects of the mesospheric Na "wall" event on October 9, 1993 during the Airborne Lidar and Observations of Hawaiian Airglow (ALOHA) campaign. Journal of Geophysical Research 103, 6361–6380.

Swenson, G.R., Haque, R., Yang, W., Gardner, C.S., 1999. Momentum and energy fluxes of monochromatic gravity waves observed by an OH imager at Starfire Optical Range, New Mexico. Journal of Geophysical Research 104, 6067–6080.

Taylor, M.J., Bishop, M.B., Taylor, V., 1995a. All-sky measurements of short period waves imaged in the OI(557.7 nm), Na(589.2 nm) and near-infrared OH and O_2 (0,1) nightglow emissions during the ALOHA-93 campaign. Geophysical Research Letters 22, 2833–2836.

Taylor, M.J., Turnbull, D.N., Lowe, R.P., 1995b. Spectrometric and imaging measurements of a spectacular gravity wave event observed during the ALOHA-93 campaign. Geophysical Research Letters 22, 2849–2852.

Tepley, C.A., Raizada, S., Zhou, Q., Friedman, J.S., 2003. First simultaneous observations of Ca^+, K and electron density using lidar and incoherent scatter radar. Geophysical Research Letters 30, 1009.

Tricker, R.A.R., 1965. Bores, Breakers, Waves and Wakes. Elsevier Science, New York 250pp.

Walterscheid, R.L., Hecht, J.H., Vincent, R.A., Reid, I.M., Woithe, J., Hickey, M.P., 1999. Analysis and interpretation of airglow and radar observations of quasi-monochromatic gravity waves in the upper mesosphere and lower thermosphere over Adelaide (35°S, 138°E). Journal of Atmospheric Solar-Terrestrial Physics 61, 461–478.

Williams, B.P., White, M.A., Krueger, D.A., She, C.Y., 2002. Observation of a large amplitude gravity wave and inversion layer leading to convective instability in the mesopause over Fort Collins, CO (41°N, 105°W). Geophysical Research Letters 29 (17), 1850.

Wu, Q., Killeen, T.L., 1996. Seasonal dependence of mesospheric gravity waves (<100 km) at Peach Mountain Observatory, Michigan. Geophysical Research Letters 23, 2211–2214.

Yamada, Y., Fukunishi, H., Nakamura, T., Tsuda, T., 2001. Breaking of small-scale gravity wave and transition to turbulence observed in OH airglow. Geophysical Research Letters 28, 2153–2156.